Escherichia coli ilvN Interacts with the FAD Binding Domain of ilvB and Activates the AHAS I Enzyme†

Ashima Mitra and Siddhartha P. Sarma*

Molecular Biophysics Unit, Indian Institute of Science, Bangalore 560012, India

Received September 16, 2007; Revised Manuscript Received October 28, 2007

ABSTRACT: The unique multidomain organization in the multimeric *Escherichia coli* AHAS I (ilvBN) enzyme has been exploited to generate polypeptide fragments which, when cloned and expressed, reassemble in the presence of cofactors to yield a catalytically competent enzyme. Multidimensional multinuclear NMR methods have been employed for obtaining near complete sequence specific NMR assignments for backbone H^N, ^{15}N, $^{13}C^{\alpha}$ and $^{13}C^{\beta}$ atoms of the FAD binding domain of ilvB on samples that were isotopically enriched in ^{2}H, ^{13}C and ^{15}N. Unambiguous assignments were obtained for 169 of 177 backbone C^{α} atoms and 127 of 164 side chain C^{β} atoms. The secondary structure determined on the basis of observed $13C^{\alpha}$ secondary chemical shifts and sequential NOEs agrees well with the structure of this domain in the catalytic subunit of yeast AHAS. Binding of ilvN to the ilvBα and ilvBβ domains was studied by both circular dichroism and isotope edited solution nuclear magnetic resonance methods. Changes in CD spectra indicate that ilvN interacts with ilvBα and ilvBβ domains of the catalytic subunit and not with the ilvBγ domain. NMR chemical shift mapping methods show that ilvN binds close to the FAD binding site in ilvBβ and proximal to the intrasubunit ilvBα/ilvBβ domain interface. The implication of this interaction on the role of the regulatory subunit on the activity of the holoenzyme is discussed.

In bacteria, as also in plants, fungi and certain algae, acetohydoxy acid synthase (AHAS) catalyzes the first step in the biosynthesis of essential amino acids isoleucine, leucine and valine (*1*−*3*). Three isoforms of AHAS (I, II and III) have been shown to be expressed in enterobacteria like *Escherichia coli* and *Salmonella (4*, *5*). Other bacterial species as well as higher organisms have been found to express a single isoform of AHAS. In *E. coli*, the induction, activity and regulation of these enzymes under differing physiological conditions are not well understood. It is known that AHAS III is expressed under normal physiological conditions whereas AHAS I is expressed under conditions of low carbon source (*6*). In spite of this, the *in vitro* enzymatic properties of the three isozymes have been extensively characterized. Biochemical characterization has been performed for both native and recombinantly expressed enzymes (*7*−*10*). Other molecular properties of the enzyme such as structure of the holoenzyme as well as the structural basis for the regulation of activity by feed back inhibition are less well understood. For instance, AHAS I is completely inhibited by valine, AHAS III is partially inhibited by valine even under saturating concentrations whereas AHAS II is insensitive to feed back inhibition by valine (*11*−*13*).

E. coli AHASs are tetrameric enzymes made up of two large and two small subunits. Components of each isozyme are coded for by pairs of linked genes, viz., *ilvBN* (AHAS I), *GM* (AHAS II) and *IH* (AHAS III) (*14*−*16*). The large subunits (∼60 kDa) are largely conserved (∼40% similarity) in all AHASs of all species. In contrast, the small subunits vary in size (10−50 kDa). For instance, ilvN of *E. coli* AHAS I is 10 kDa (*17*), ilvH of AHAS III is 18.0 kDa (*18*), the regulatory subunit of yeast AHAS is 40 kDa (*19*) and that of *A. thaliana* is 52 kDa (*20*). *E. coli* AHAS III appears to have greatest commonality with other bacterial AHASs when sequence and size of large and small subunits are both taken into consideration (*21*). All AHASs require TPP[1] and FAD cofactors for catalytic activity. The catalytic site is present in the large subunit, while the small subunit performs a regulatory function in all known AHASs. Maximum activity is obtained for the holoenzyme and the activity drops to ∼15% in the absence of the regulatory subunit.

The structure of the dimeric catalytic subunit of yeast AHAS (in the presence of cofactors) has been determined by Duggleby and co-workers (*22*, *23*). The structure shows that each catalytic subunit is folded into three distinct domains (called α, β and γ) and that the active site is formed at the inter-subunit interface, in which the α-domain of one subunit complexes with the γ-domain of the second subunit to form the catalytic site. This is a unique feature of the catalytic site of AHAS since the α and γ domains possess group specific binding sites for the cofactor TPP (*22*). The dimeric structure of the regulatory subunit (ilvH) of *E. coli* AHAS III has also been determined using X-ray crystal-

† A.M. is a recipient of a CSIR−UGC NET fellowship. S.P.S. thanks DBT, India, for financial support.

* To whom correspondence should be addressed: Siddhartha P. Sarma, 207, Molecular Biophysics Unit, Indian Institute of Science, Bangalore, 560012. Tel: 91-80-22932839. Fax: 91-80-23600535. E-mail: sidd@mbu.iisc.ernet.in.

[1] Abbreviations: TPP, thiamin pyro-phosphate; FAD, flavin adenine dinucleotide; IPTG, isopropyl β-D-1-thiogalactopyranoside; Tris, trishydroxymethylaminomethane; IMAC, immobilized metal ion affinity chromatography; EDTA, ethylene diamine tetraacetic acid; DTT, dithiothreitol; DPC, dodecylphosphocholine; DSS, sodium 4,4-dimethyl-4-silapentanesulfonate; HSQC, heteronuclear single quantum coherence; TROSY, transverse relaxation optimized spectroscopy; CHAPS, 3-[(3-cholamidopropyl)dimethylammonio]-1-propanesulfonate.

10.1021/bi701893b CCC: $40.75
Published on Web 01/15/2008

lography by Chipman, Barak and co-workers (*24*). Mutagenic studies on ilvH have shown that the N-terminal domain of this subunit is responsible for dimerization and also for activation of the catalytic subunit (*24*−*26*). Based on these studies and on the homology of the ACT domain of ilvH with the regulatory subunit of 3PGDH, a binding site for the effector, in this case valine, has also been proposed (*24*, *25*).

The structural basis for the interaction of the small subunit with the large subunit in the case of AHAS I is not known. In a manner similar to ilvH, ilvN may interact with ilvB as a dimer. Knowledge of this interaction is important for understanding the factors that control enzyme activity in terms of catalytic efficiency as well as the regulation by feed back inhibition. To date there have been no reports on successful crystallization of the holoenzyme. An active AHAS I construct has been created by Vyazmensky et al., where the catalytic and the regulatory subunit have been expressed together as a single chain separated by a flexible linker (*27*). While this single chain construct is catalytically active, there have been no reports of successful crystallization of this single chain AHAS I enzyme. The unique domain architecture of the AHAS catalytic subunit and the relatively small size of the regulatory subunit form the basis for implementation of a novel strategy, in which structural interactions between the domains (catalytic site as well as the noncatalytic site interactions) as well as structural interactions between the domains of the catalytic and the regulatory subunit can be explored in an incremental manner.

We have initiated structural studies on these interactions employing solution NMR methods in addition to other spectroscopic and biochemical methods.

As a first step we report the cloning, expression and purification of the α, *β* and *γ* domains (henceforth referred to as ilvBα, ilvB*β* and ilvB*γ*, respectively) of the catalytic subunit as well as the regulatory subunit (ilvN) of *E. coli* AHAS I. Multinuclear, multidimensional solution NMR methods have been utilized to obtain sequence specific assignments and secondary structure of the non FAD bound (apo) form of ilvB*β*. Using chemical shift mapping methods, the residues of the ilvB*β* domain that are involved in FAD binding have been identified. In addition we also show that reconstituted domains form a catalytically competent enzyme and that the regulatory subunit interacts specifically with the ilvB*β* and ilvBα domains of the catalytic subunit.

MATERIALS AND METHODS

Identification of Domains within E. coli ilvB. Sequence alignment of template and target proteins was performed using the Bestfit routine in the GCG (version 10.3-UNIX) software package (http://www.accelrys.com/products/gcg/). The N- and C-termini of the α, *β* and *γ* domains of *E. coli* ilvB were identified using the available structural information of the yeast AHAS (PDB ID: 1JSC).

*Cloning and Protein Expression. Cloning of ilvBα, ilvB*β *and ilvB*γ. Specific primers were designed to PCR amplify the coding regions of these domains in the *ilvB* gene from *E. coli* genomic DNA. The amplified product was ligated into an appropriately digested pet21a plasmid vector to yield the clone ilvBα. The *β* and *γ* domains of ilvB as well as ilvN were cloned as cytb5 based fusion proteins. The cloning strategy and purification protocol of the fusion proteins have been described elsewhere (*28*).

Protein Expression. All proteins were expressed using *E. coli* BL21 (*DE3*) as host strains. Unless specified, cells were grown in Luria broth and protein production was induced by addition of IPTG to a final concentration of 0.5 mM. Cells were harvested by centrifugation and lysed using a French Press and cell debris was removed by centrifugation.

Purification of ilvBα. Ammonium sulfate was added to the lysate supernatant to a final concentration of 60%, and the solution was kept on ice for 1 h. The precipitate (ilvBα) was centrifuged at 3075*g* for 20 min. The pellet was resolubilized in 20 mM Tris buffer (pH 7.4) and dialyzed against the same buffer. The dialysate was loaded onto an IMAC (Ni^{2+}) affinity column. The protein bound column was washed with 5 volumes of binding buffer, following which bound protein was eluted using a 0−1 M linear imidazole gradient. The purified protein was dialyzed into 20 mM potassium phosphate buffer, pH 7.0, containing 20 mM NaCl, 1 mM DTT and 1 mM EDTA.

Thrombin Digestion. Cleavage of target proteins from the fusion host was achieved by dialyzing the fusion proteins into the thrombin cleavage buffer (50 mM Tris, pH 8.0, 100 mM NaCl and 5 mM $CaCl_2$). Thrombin digestion was accomplished by using 1 unit of the protease for each milligram of fusion protein. The cleavage reaction was performed at 22 °C for 16 h.

*Separation of ilvB*β*, γ and ilvN from Fusion Host.* The cleaved ilvB*β* was separated from the fusion host by ammonium sulfate precipitation (60% saturation). The precipitate (ilvB*β*) was washed twice with 60% saturated solution of ammonium sulfate to remove any trace of cytb5. The pellet was subsequently resolubilized in 20 mM potassium phosphate buffer (pH 7.0) containing 20 mM NaCl, 1 mM EDTA and 2.5 mM DTT. The *γ* domain of ilvB and ilvN were separated from the fusion host by gel filtration chromatography using a S-100 16/60 sephacryl column (Pharmacia) and dialyzed into appropriate buffer.

*Preparation of Isotopically Enriched Samples of ilvB*β *and ilvB*α. Uniformly ^{15}N enriched samples of ilvB*β* and ilvBα were prepared by growing cells in minimal (M9) medium supplemented with $^{15}NH_4Cl$ (1 g L^{-1}) (Isotec) as the sole nitrogen source. $^{13}C/^{15}N$ enriched sample of ilvB*β* was made by growing cells in $^{13}C/^{15}N$ ISOGRO (Isotec) medium reconstituted by dissolving 5 g of ISOGRO powder into 500 mL of water. Deuterated ($^{13}C/^{15}N/^{2}H$) sample of the protein was prepared by growing cells in $^{2}H/^{13}C/^{15}N$ labeled ISOGRO (Isotec) medium. Samples of ilvB*β* for NMR were prepared after diluting the protein 10-fold into 20 mM sodium acetate buffer(pH 5.2) containing 50 mM arginine, 50 mM glutamate, 20 mM proline, 0.6 mM DPC, 1 mM EDTA, 20 mM NaCl and 0.01% NaN_3 followed by concentration to a volume of 1.5 mL. The protein concentration was estimated by measuring UV absorbance at 280 nm using the calculated extinction coefficient of 8.2 mM^{-1} cm^{-1}.

NMR sample of ilvBα was prepared in 20 mM potassium phosphate buffer (pH 7.0) containing 50 mM arginine, 50 mM glutamate, 20 mM proline, 0.6 mM DPC, 1 mM EDTA, 20 mM NaCl and 0.01% NaN_3 after repeated rounds of dilution and concentration.

*Preparation of ilvB*β *and ilvB*α *for Interaction Studies with the Regulatory Subunit.* Interaction studies of ilvB*β* and

ilvBα with ilvN were performed in 20 mM potassium phosphate buffer (pH 7.0) containing 50 mM arginine, 50 mM glutamate, 20 mM NaCl, 2.5 mM DTT, 20 mM proline, 1 mM EDTA and 0.01%NaN_3. The regulatory subunit was added in a molar ratio of 2:1 to ilvBβ or ilvBα, the mixture was diluted to a volume of 30 mL in the same buffer and coconcentrated to a volume of 1.5 mL.

NMR Spectroscopy. All NMR spectra were acquired on a Bruker-Avance spectrometer operating at a proton frequency of 700 MHz equipped with a 5 mm triple resonance cryoprobe with single (*z*-axis) pulsed field gradient accessory. NMR spectra were acquired at 300 K. Protein samples for NMR spectroscopy were prepared in buffers made in 90% H_2O:10%D_2O at a concentration of 0.15−0.20 mM. Two-dimensional $^1H-^{15}N$ HSQC spectra were acquired using the WATERGATE sequence for solvent suppression (*29*, *30*).

Triple resonance data sets were acquired using sensitivity enhanced TROSY versions of the triple resonance experiments (*31*−*37*). Quadrature detection in the carbon (F1) dimension was achieved using the STATES-TPPI method (*38*). Quadrature detection in the ^{15}N (F2) dimension was achieved through recording Echo and AntiEcho coherences using pulsed field gradients. 3D ^{15}N-NOESY-HSQC (200 ms mixing time) was acquired with pulse program that incorporated Watergate solvent suppression scheme (*39*). A list of NMR experiments and data acquisition parameters is tabulated in Table S-1 (Supporting Information).

NMR data were processed on an INTEL PC workstation running on Suse Linux 10.0 using NMRPipe/NMRDraw processing software (*40*). The directly and the indirectly detected time domain data of 2D and 3D spectra were processed by applying a 90° phase-shifted squared sine bell filter. Data sets were zero filled in each dimension prior to Fourier transformation. All chemical shifts were referenced to external DSS. The NMR spectra were analyzed using ANSIG (*41*, *42*).

All three-dimensional structures were visualized using the molecular graphics programs VMD or MOLMOL (*43*, *44*).

Circular Dichroism Spectroscopy. All CD spectra were acquired on a JASCO-715 spectropolarimeter. Spectra (averaged over 4 scans) were recorded in a wavelength range of 300−190 nm at a scan rate of 100 nm min^{-1} using a 2 mm path length cuvette. Proteins used for CD studies were prepared in 50 mM potassium phosphate buffer (pH 7.6) containing 100 mM KCl and 1 mM EDTA. The concentrations of the proteins were in the range of 20−25 μM.

Mass Determination. Electrospray ionization mass spectra were acquired on a Bruker Daltonics Ultraflex mass spectrometer. The samples were infused into the mass spectrometer through a reverse phase C18 column (Zorbax, 4.6 × 150 mm) by application of gradient elution using a binary solvent system (solvent A, 0.1% acetic acid in water, and solvent B, 0.1% acetic acid in acetonitrile) at a flow rate of 1.00 mL min^{-1}.

Enzyme Activity. All enzyme reactions were carried out as described earlier (*12*). The assays were performed in 50 mM potassium phosphate buffer, pH 7.8, containing 100 mM KCl, 1 mM DTT, 100 mM $MgCl_2$, 1.0 mM TPP, 0.075 mM FAD with each domain added to a final concentration of 50 μM. Increasing concentrations of pyruvate were added to the reaction mixtures. The reactions were performed at 37 °C and quenched at the end of 14 h of incubation. The acetolactate formation was determined by the method of Westerfeld (*45*, *46*). Circular dichroism spectroscopy and NMR spectroscopy were also used to identify product formation (*47*, *48*).

RESULTS

Identification of Domains of E. coli ilvB. The three domains of the *E. coli* catalytic subunit were identified to span residues 1−186 (ilvBα), residues 187−359 (ilvBβ) and residues 360−564 (ilvBγ).

Protein Expression and Purification. The domains of ilvB as well as ilvN express to high levels (Figure S-1a, Supporting Information). The advantages of the cytb5 fusion protein system for high level expression of heterologous proteins have been shown previously (*28*). Purification of fusion proteins was accomplished using protocols previously described. Duggleby and co-workers have shown that AHAS itself binds to metal affinity columns (*8*). We have found that all three domains of ilvB as well as ilvN bind to metal chelated columns. Using this property, purification of ilvBα was accomplished in a simple two step procedure. Use of metal affinity chromatography to separate ilvBβ, ilvBγ and ilvN from the fusion host, after treatment with protease, was hampered by the fact that apocytochrome b_5 itself binds to metal chelated columns. Thus ammonium sulfate precipitation and/or gel filtration was the method of choice to achieve separation of ilvBβ, ilvBγ and ilvN from the fusion host. The ilvBβ domain expressed as a cytochrome b_5 fusion was obtained in a non FAD bound form and was purified as such (Figure S-1b).

Mass Determination. Mass spectrometric analysis has shown that individual proteins are expressed to full length (Figure 1). The measured masses of ilvBα and ilvBβ correspond exactly to the calculated masses for these proteins. In the case of ilvN and ilvBγ the measured mass is in excess by 49 Da for the former and 19 Da for the latter. Sequencing analysis has shown that ilvN contains an N → Y mutation. The nature of the mutation in the case of ilvBγ is yet to be ascertained. These mutations in ilvN and ilvBγ appear to have no effect on the activity of the enzyme (*vide infra*).

NMR Studies. Solution Properties of apo-ilvBβ. Initial NMR studies of ilvBβ (in potassium phosphate buffer, pH 7.0), showed that this domain existed in equilibrium between monomeric and higher oligomeric species. Several buffer conditions were explored in an attempt to improve the quality of the NMR spectrum. Addition of cofactors (TPP and FAD), substrate (pyruvate) and valine had no effect on the spectrum. Addition of protein stabilizers such as arginine and glutamate improved the spectrum marginally (*49*). Addition of CHAPS had no effect on the spectrum (*50*). Replacement of CHAPS with DPC improved the spectrum. Change to an acidic buffer pH 5.2 (20 mM sodium acetate) also improved the spectrum which is reflected by an improvement in concentration and chemical shift dispersion. A dramatic change in the quality of the spectrum was witnessed upon addition of proline to the sample buffer in terms of chemical shift dispersion and also as an increase in concentration. However, we were unable to obtain protein sample concentrations >0.2 mM even under these conditions. Thus all ilvBβ samples for obtaining resonance assignments were prepared in the buffer as described in Materials and Methods. Figure S-2 catalogues

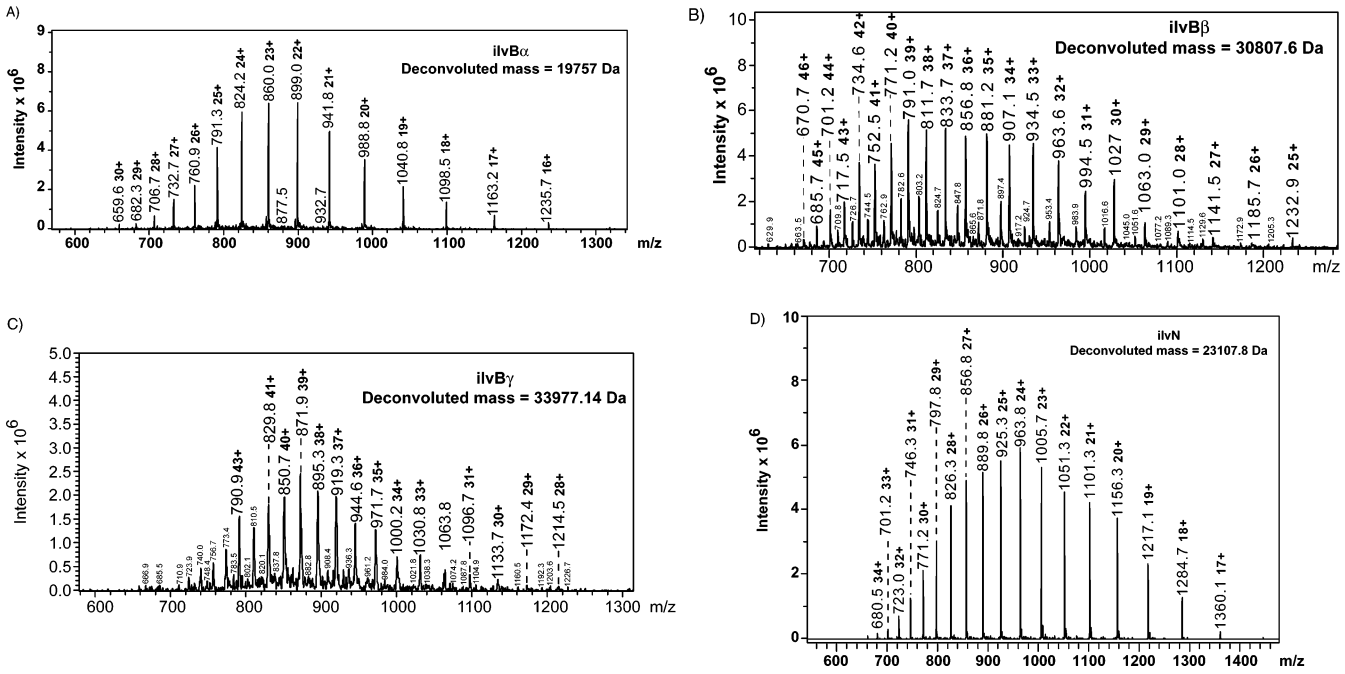

FIGURE 1: LC−ES-MS spectra of (A) ilvBα, (B) cytb5−ilvB*β*, (C) cytb5−ilvB*γ*, and (D) cytb5−ilvN. The deconvoluted mass is indicated in the upper right-hand corner in each spectrum. See text for details.

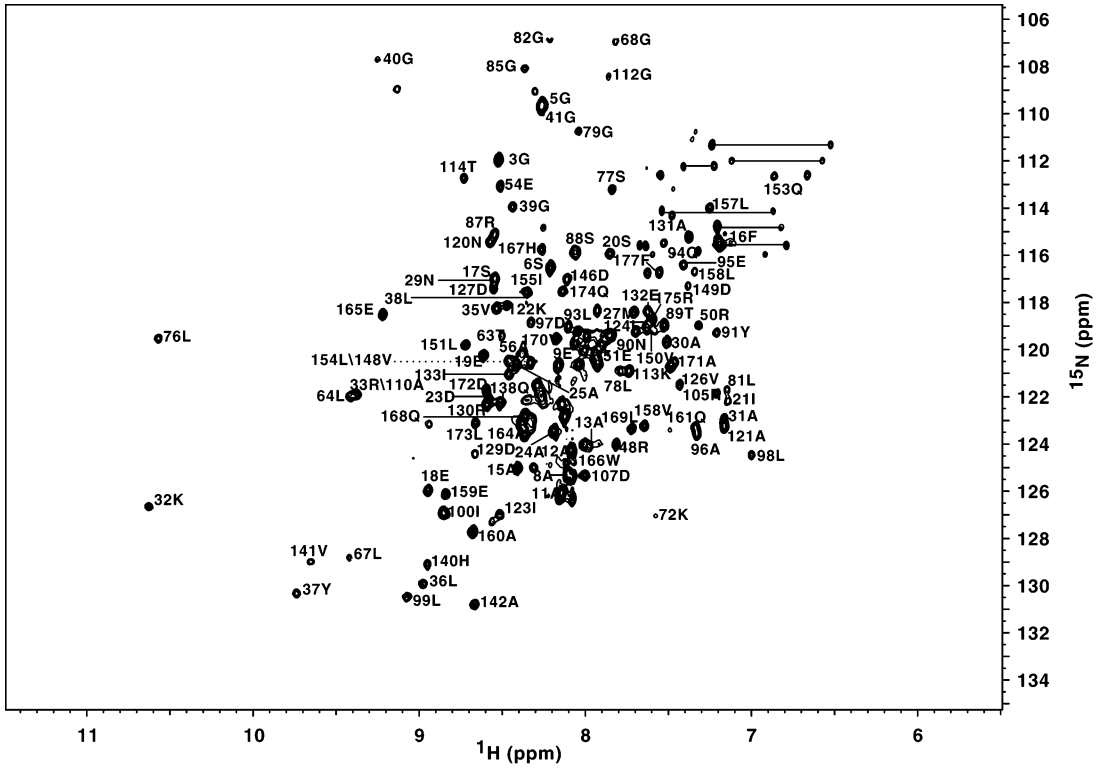

FIGURE 2: Two-dimensional ^{1}H−^{15}N HSQC spectrum of the 178 residue apo-ilvB*β* domain. Indicated on the spectrum are sequence specifically assigned backbone amide proton−amide nitrogen pairs. For clarity only resolved resonances have been labeled. Pairs of correlation peaks arising from side-chain amides of asparagine and glutamine are connected by horizontal lines.

the effects of the various additives on the quality of the spectrum of ilvB*β*. For studies of the interaction of ilvB*β* with ilvN, the samples were prepared in similar solution conditions except that the acetate buffer was replaced with 20 mM potassium phosphate buffer, pH 7.0.

*Solution Properties of ilvB*α. ilvBα was also found to exist as equilibrium mixture between oligomeric states in 20 mM potassium phosphate buffer, pH 7.0, containing 20 mM NaCl, 1 mM DTT and 1 mM EDTA. Here too addition of proline to the sample buffer dramatically improved the quality of the spectrum.

Sequence Specific Assignments of apo-ilvBβ. ilvB*β* has in its sequence eighteen alanines of which two triplet stretches are present in the N-terminal region of the protein. The sequence also has a glycine triplet. Furthermore, the triplet sequence of LGM (leucine-glycine-methionine) occurs thrice in the N-terminal region of the protein of which two of the repeats are sequential, making sequence specific

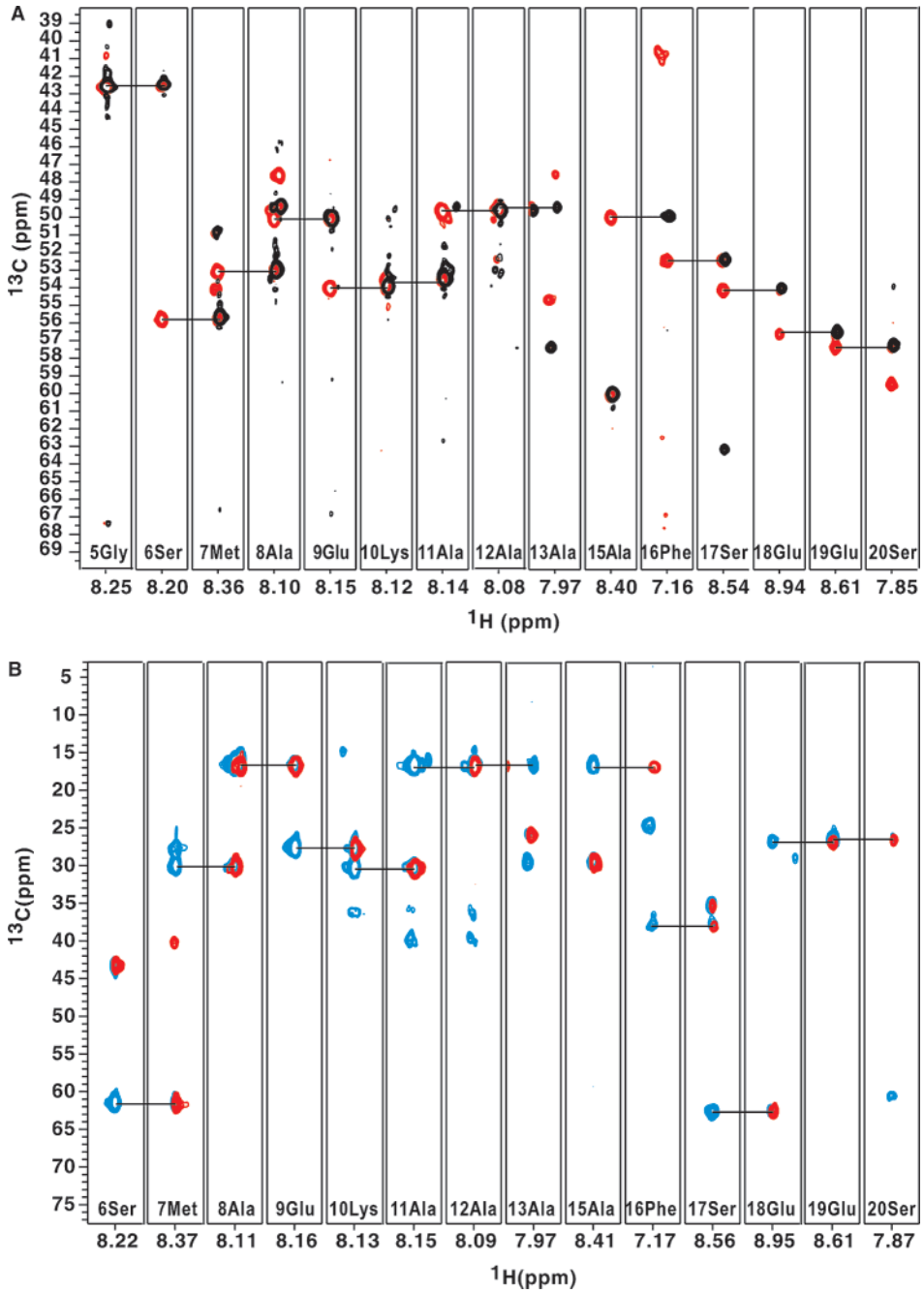

FIGURE 3: Sequential connectivity walk along the protein backbone for residues 5−20 of apo-ilvBβ. (A) Overlay of strip-plots from the 3D HNCA (red) and HN(CO)CA (black) spectra showing intraresidue and interresidue C$^{\alpha}$ correlations for the residues indicated above. A break in the sequential connectivity is witnessed at residue 14, which is a proline. (B) Overlay of strip-plots from the 3D HN(CA)CB (blue) and HN(COCA)CB (maroon) spectra showing intra- and interresidue C$^{\beta}$ correlations for the residues indicated above.

assignments of this region of the protein extremely difficult. In addition, the low sample concentration employed in these studies proved to be a bottleneck in our attempt to obtain structural restraints that would enable a high-resolution three-dimensional structure determination under solution conditions. Such a structure determination has been possible for other proteins of comparable size (*51*−*54*). Figure 2 shows the sequence specifically assigned ^{1}H−^{15}N HSQC of apo-ilvBβ. The HSQC spectrum exhibits well-resolved resonances for nearly all backbone and side chain proton nitrogen pairs. Initial attempts to obtain triple resonance data sets using protonated samples of ilvBβ were unproductive due to poor coherence transfer in the experiments that correlate C$^{\beta}$ chemical shifts either alone or in addition to the C$^{\alpha}$ chemical

Table 1: Comparison of Secondary Structure Elements in ilvBβ of *E. coli* and Yeast AHAS

	E. coli	yeast
α-helix		
I	13−30	282−298
II	47−54	316−326
III	87−94	358−366
IV	148−154	427−435
V	165−176	445−455
β-strands		
I	37−44	302−306
II	60−62	331−333
III	77−80	348−351
IV	124−127	369−373
V	141−144	402−406

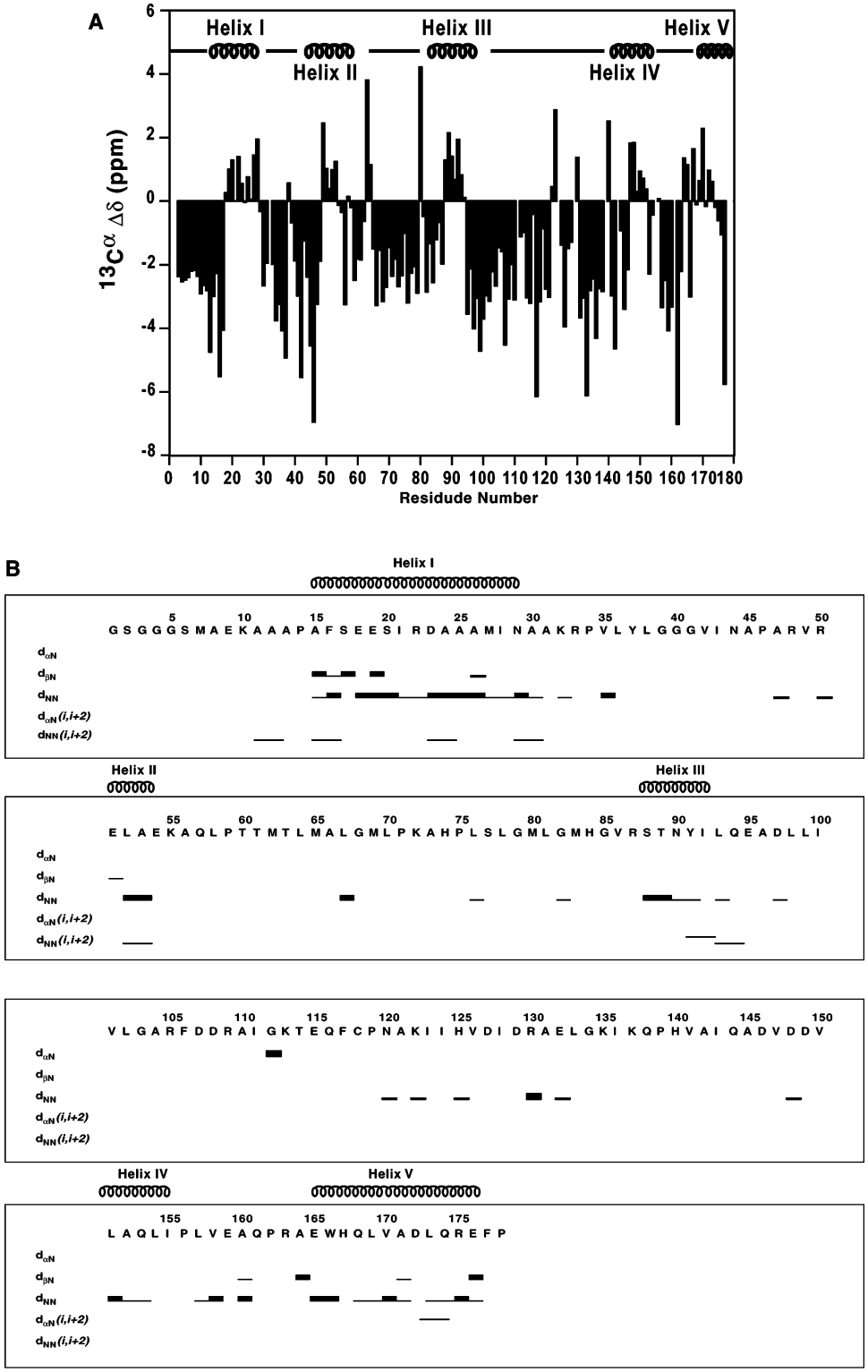

FIGURE 4: (A) $^{13}C^{\alpha}$ secondary chemical shifts as a function of residue number for apo-ilvBβ domain. Shown in the figure is the distribution of the secondary structural elements with the image of a coil representing a helix and a boldface horizontal bar representing a β-sheet. (B) Summary of sequential NOEs assigned in 3D ^{15}N-edited NOESY-HSQC spectrum of ilvBβ.

shifts with amide proton−nitrogen pairs. Sequence specific assignments were possible only through the use of uniformly ^{2}H, ^{13}C and ^{15}N labeled samples, using which the C$^{\beta}$ chemical shift correlation experiments could be recorded. Thus sequence specific assignments were obtained through analysis of HNCA/HN(CO)CA and HN(CA)CB/HN(COCA)CB spectra (*31*). Figures 3A and 3B show plots of the sequential assignment of residues 4−20 in the N-terminal region of the protein. Using these spectra we were able to obtain backbone (H^{N}, N, C$^{\alpha}$ and C$^{\beta}$) resonance assignments for ~92% of the residues. In several instances the missing cross peaks for *i* − 1 residues in the HNCA and HNCACB spectra were assigned on the basis of cross peaks present in the HN(CO)-CA and HN(CO)CACB spectra. One hundred fifty-six of the expected 177 C$^{\alpha}$ correlations could be assigned unambiguously in the HNCA spectrum. An additional 13 C$^{\alpha}$

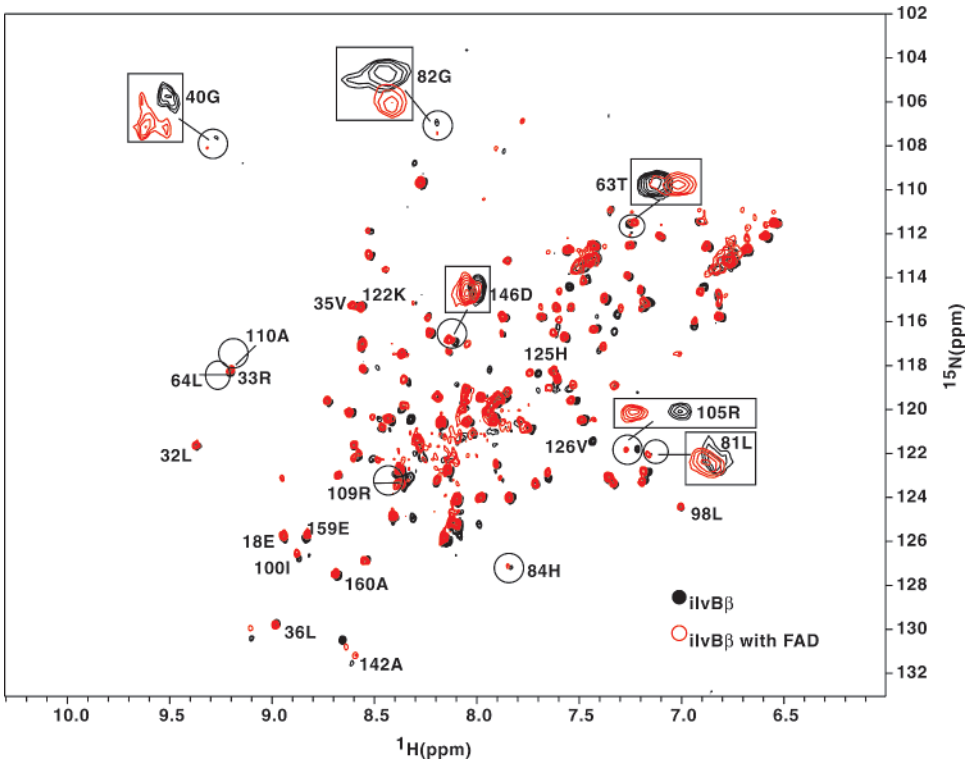

FIGURE 5: An overlay of 2D ^{1}H−^{15}N HSQC spectra of ilvBβ acquired in the absence (black) and presence (red) of FAD. FAD was added to a final concentration of 1 mM. Residues that exhibit significant changes in chemical shift upon binding FAD have been mentioned in the text. Expanded views are shown for residues G40, T60, L81, G82, 105R and 146D. The resonances corresponding to residues L64, R109 and A110 are missing in the FAD bound spectrum and are represented by open circles.

resonances were assigned using the data from the HN(CO)-CA spectrum. Similarly 104 of expected 164 C$^{\beta}$ atoms were assigned using the data obtained from HN(CA)CB spectrum and an additional 23 C$^{\beta}$ atoms were assigned using the data obtained from HN(COCA)CB spectrum. Thus ~92% of backbone C-alpha atoms and ~76% of side chain C-beta atoms were assigned unambiguously. All ^{13}C$^{\alpha}$ and ^{13}C$^{\beta}$ correlation were missing for residues V125 and H126. These residues were assigned on the basis of observation of sequential NOEs in the ^{15}N-edited 3D-NOESY-HSQC spectrum.

Identification of Secondary Structural Elements. The secondary structure of apo-ilvBβ was assigned on the basis of ^{13}C$^{\alpha}$ secondary chemical shifts as well as from backbone−backbone sequential NOEs (*55*). The secondary structural elements are distributed in alternating stretches of alpha helical and beta sheet regions. Five alpha helices were identified with the smallest helix containing eight residues and the longest containing as many as eighteen residues. Table 1 lists the secondary structural elements in *E. coli* ilvBβ as a function of sequence. For comparison, the secondary structural elements in the yeast ilvBβ-domain are also listed. Figure 4A shows the difference in observed ^{13}C$^{\alpha}$ secondary chemical shifts and Figure 4B summarizes the short and medium range NOEs observed in the ^{15}N-edited 3D-NOESY-HSQC spectrum. The distribution of the secondary structural elements is also denoted in the figure. The secondary structure of *E. coli* ilvBβ domain in solution differs from the crystallographically determined structure of the yeast protein, in that the *E. coli* protein has 5 fewer helices. In the yeast structure, three of these helices are identified as 3_{10} helices and these could not be identified in the *E. coli* protein. Also missing in the *E. coli* protein are two regular α-helices, corresponding to residues 379−382 and 390−397 in the yeast structure. Of these, the residues in the 379−382 region are involved in FAD binding in the yeast structure (*vide infra*) and thus the observed differences in secondary structure may reflect differences in the structure of the apo and holo forms of ilvBβ. On the otherhand, residues 390−397 that are present in the yeast protein are missing in the *E. coli* protein (*cf.* Figure 9).

Interaction of ilvBβ with FAD. Figure 5 shows an overlay of the ^{1}H−^{15}N HSQCs of the apo and holo forms of the ilvBβ domain. The residues which exhibit marked chemical shift changes upon binding FAD are G40, T63, L64, L81, G82, R105, R109, A110 and D146. Inspection of the sequence and structure of the ilvBβ domain of the yeast catalytic subunit shows that the residues that are involved in FAD binding are conserved in sequence in the two proteins. Furthermore these residues also occur in the same secondary structural elements in the two proteins. This strongly suggests that, in the FAD bound form, the two proteins have near identical tertiary structures. In addition residues K122, I123, H125 and V126 which are not directly involved but lie close to the FAD binding region also exhibit chemical shift changes.

Interaction Studies of ilvN and the Domains of ilvB. Enzyme Activity. The ilvBα and ilvBγ complex should in principle represent the minimal active site of AHAS. The effect of addition of ilvBβ and ilvN individually and in combination on the activity of the enzyme was then examined. Formation of acetolactate was confirmed by one-dimensional NMR spectroscopy following which product formation was monitored by a colorimetric method. Figure 6A shows the one-dimensional NMR spectrum of the products observed for the reaction catalyzed by the ilvBα−

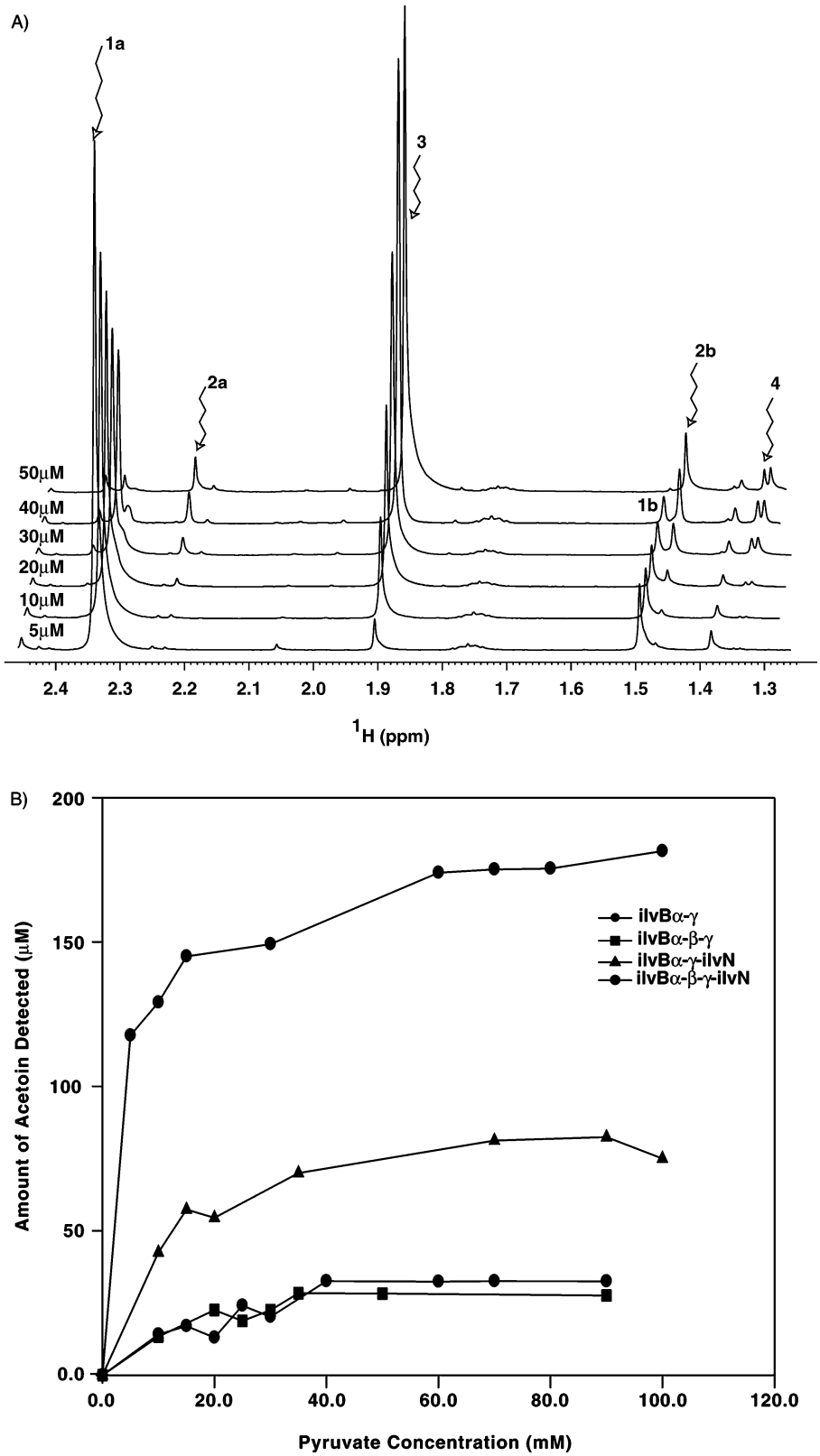

FIGURE 6: (A) A stack plot of one-dimensional NMR spectra showing product formation as a function of the enzyme complex composed of ilvBα−γ−ilvN at a fixed pyruvate concentration of 40 mM. The conversion of pyruvate (peaks 1a,b) to acetolactate (peaks 2a,b), and acetate (peak 3) can be observed with the increase in enzyme concentration. Acetoin (peak 4) was also identified as one of the products of the enzyme reaction. (B) Plot comparing the amount of acetolactate formed as a function of substrate concentration. The domain composition for each reaction is indicated in the figure. Acetolactate was estimated by the Westerfeld method.

ilvBγ−ilvN complex at increasing enzyme concentration and fixed concentration of substrate. The NMR spectrum shows conversion of pyruvate (s, δ 2.35 ppm) to acetate (s, 1.92 ppm) and acetolactate (s, 2.26 ppm and 1.46 ppm). Chemical shift assignments are based on recorded chemical shifts of pure samples of pyruvate, acetate and acetoin. Assignments of resonances originating from acetolactate agree with values reported in literature (*48*). At an enzyme concentration of

50 μM of each component, near complete conversion of pyruvate into products was observed. The presence of acetoin in the spectrum is presumably due to conversion of acetolactate to acetoin during NMR data acquisition. Formation of acetate from pyruvate results from an oxygenase side reaction catalyzed by enterobacterial AHASs. The identification of acetate in the NMR spectrum suggests that the similar side reaction is also catalyzed by the assembled enzyme described above (*12*, *56*, *57*).

Figure 6B shows the formation of product as a function of substrate concentration, for different domain and subunit compositions of AHAS I. In the colorimetric reaction carried out here, arginine and α-naphthol were added in fixed amounts to each reaction. Thus the amount of acetoin detected does not reflect the total acetoin in the product. Nevertheless it is clear that the quantity of product formed is a function of the domain and subunit composition in the enzyme reaction. The ilvBα and γ complex was found to be enzymatically active. The addition of ilvBβ or ilvN increased the activity of the complex marginally. A dramatic increase in activity was observed for an enzyme complex composed of all three domains of ilvB and ilvN, upon reconstitution.

Acetolactate formed in the reaction shows a positive Cotton effect in the CD spectrum (Figure S-3) providing strong evidence that the product is of the same absolute configuration as the one produced by native AHAS I (*47*).

Circular Dichroism Studies. Figure 7A shows the CD spectrum of the regulatory subunit in the presence of individual domains of ilvB. Overlaid in each spectrum are the spectra of individual components of the mixture. Furthermore the calculated spectrum that would result from individual contributions of each component of the complex in the absence of physical interaction is also shown.

Qualitative changes in the CD spectrum of the ilvBα−ilvN spectrum and the ilvBβ−ilvN spectrum strongly suggest that the regulatory subunit interacts with these two domains of the catalytic subunit. In the case of the interaction of ilvBγ with ilvN, it can be observed that the measured spectrum has a near identical profile with that of the computed spectrum, notwithstanding changes in intensity due to dilution effects. This is strong evidence that the regulatory subunit does not interact with the ilvBγ domain.

CD spectrum of the resulting complex when all domains of ilvB and the regulatory subunit are reconstituted is similar in form (Figure 7B) to the CD spectrum of the holoenzyme of AHAS II (*8*)

NMR Studies of Interaction of ilvN with ilvBβ and ilvBα. Interaction studies of ilvN with ilvBβ and ilvBα were performed in phosphate buffer at pH 7.0. The regulatory subunit has extremely low solubility at pH 5.2. Figure 8A shows an overlay ^{15}N filtered HSQC spectrum of ilvBβ in the presence and absence of ilvN. Such a direct comparison of spectra should enable identification of backbone proton−nitrogen pairs of residues in ilvBβ that are involved in binding interactions with ilvN as these residues are expected to exhibit changes in chemical shift. On this basis we have been able to confidently identify six residues that exhibit discernible shifts for amide protons (>42 Hz, digital resolution 2.4 Hz/Point). These residues are 18E, 140H, 145A, 147V, 148D and 150V.

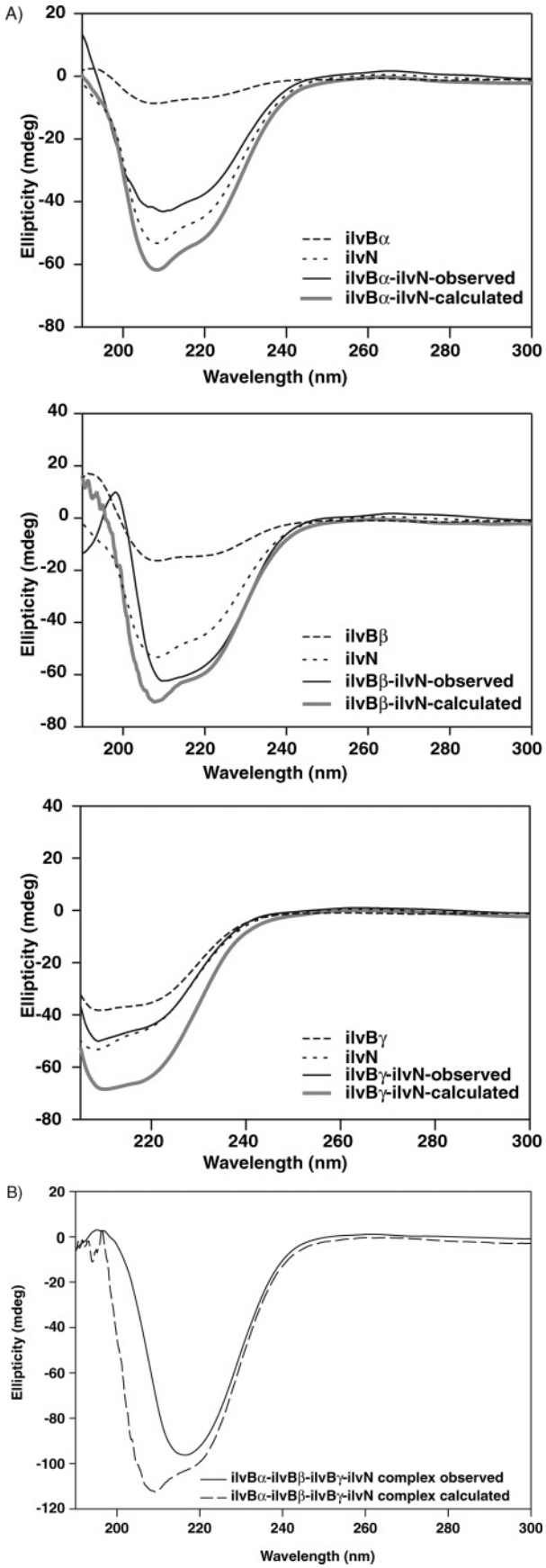

FIGURE 7: (A) CD spectrum of the ilvBα, ilvBβ and ilvBγ upon complexation with ilvN. Overlaid are the spectra of the individual components as well as the calculated spectrum of the mixture. (B) CD spectrum of the assembled enzyme prepared by reconstituting the three domains as well as ilvN. Each protein was added to a final concentration of 20 μM.

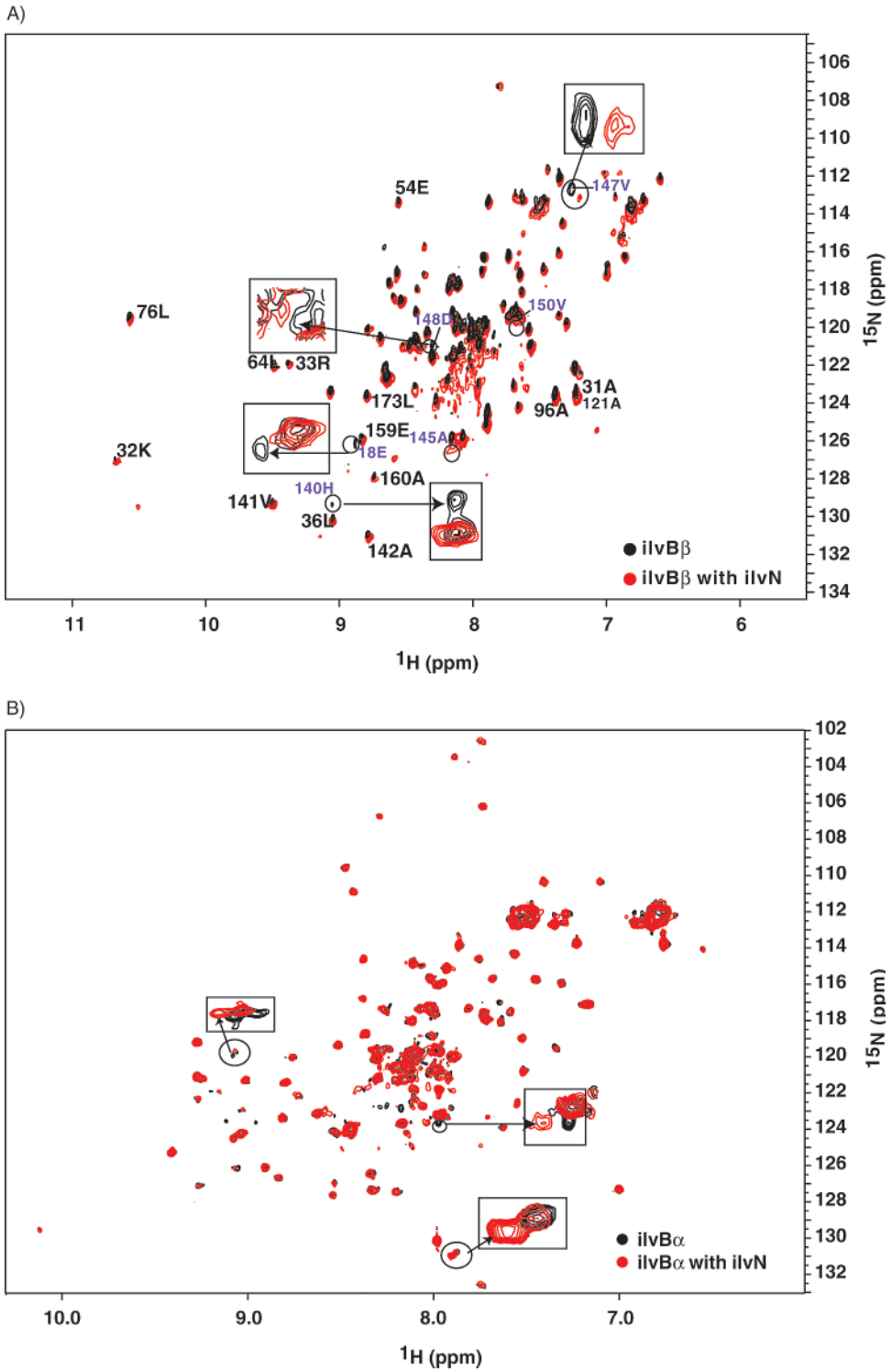

FIGURE 8: (A) An overlay of 2D $^{1}H-^{15}N$ HSQC spectrum of ilvBβ in the absence (black) and presence (red) of ilvN. The residues that show changes in chemical shift have been mentioned in the text. Expanded views have been shown for the residues 18E, 140H, 147V and 148D. (B) An overlay of 2D $^{1}H-^{15}N$ HSQC spectrum of ilvBα acquired in the absence (black) and presence (red) of ilvN. Expanded views have been shown for the three residues that show changes in chemical shift. Sequence specific assignments of ilvBα have not been made.

In the case of the interaction of ilvN with ilvBα, we have observed changes in the chemical shifts for three backbone amide proton and amide nitrogen pairs (Figure 8B). It should be noted that sequence specific assignments for the ilvBα domain have not yet been made. However given the small changes in the CD spectrum of the ilvBα/ilvN complex, we expect fewer changes in the NMR spectrum of ilvBα in the presence of ilvN.

Site of Interaction of ilvN with ilvBβ. Figure 9A shows the sequence comparison of the ilvBβ domains of *E. coli* and yeast AHAS I. Marked on the sequence are the residues in each protein that are involved in FAD binding as well as the residues that are involved in binding the regulatory subunit in the *E. coli* protein. Figure 9B shows the structure of the yeast ilvBβ domain. We have used the crystal structure of the yeast catalytic subunit to depict the region of binding

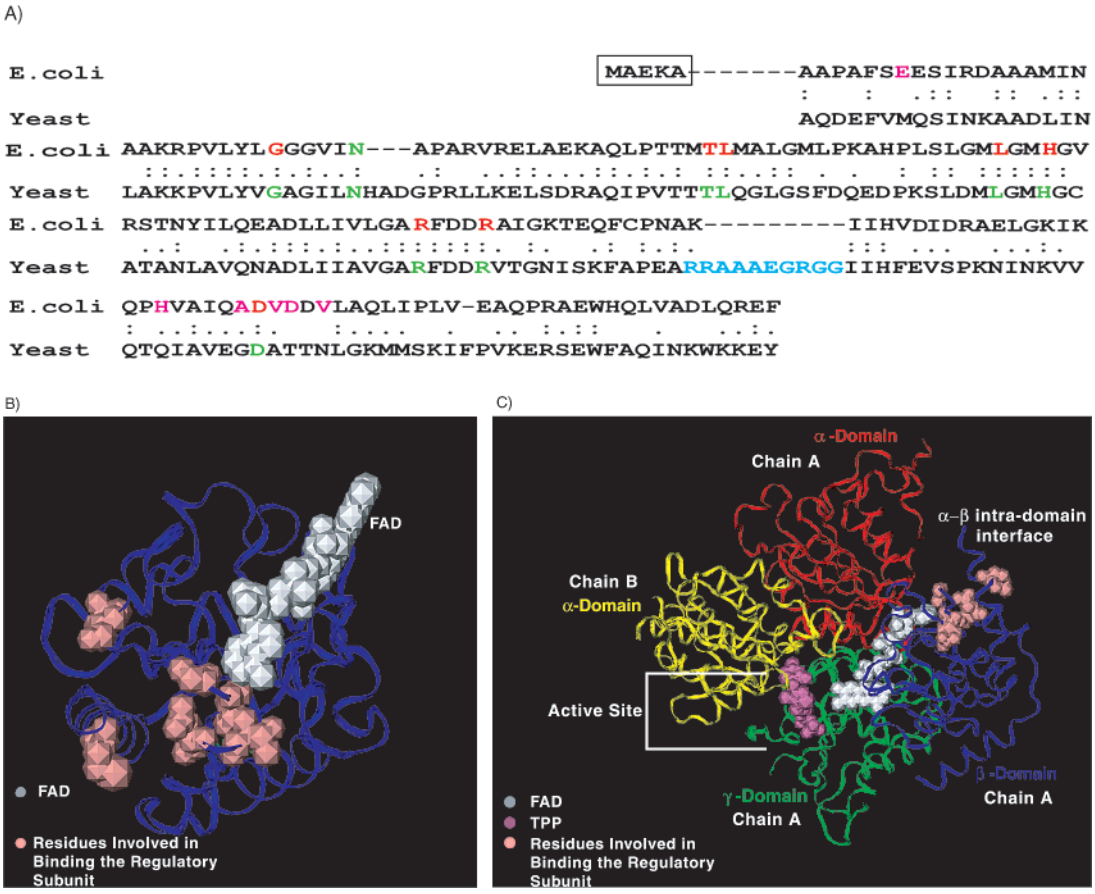

FIGURE 9: (A) Sequence alignment of ilvBβ with the FAD binding β domain of yeast AHAS. The two domains share a sequence similarity of 55% and an identity of 40%. The ilvBβ has five extra residues which are enclosed in a rectangular box. The residues involved in binding FAD are conserved (represented in red and green for *E. coli* and yeast, respectively). The extra residues of the β-domain of the yeast protein which form a helix are denoted in blue. The residues of ilvBβ involved in binding ilvN have been represented in pink. (B) A ribbon representation of the β domain of yeast AHAS. The residues of the yeast protein that correspond to the residues of ilvBβ that exhibit changes in chemical shift upon binding ilvN are represented in pink (space filled models). These residues include 286M (18E), 420Q (140H), 425G (145A), 427A (147V), 428T (148D) and 430N (150V). The residues appear in the identical secondary structural regions of the two proteins. (C) A ribbon representation of the three-dimensional structure of the yeast catalytic subunit. The active site is located at the inter-subunit α (yellow)/γ (green) domain interface and can be identified by the presence of a TPP (mauve) molecule. Residues (pink) involved in binding ilvN lie at the intra-subunit α (red)/β (blue) domain interface at a close proximity to the FAD (white) binding region of the β domain.

of ilvN to the catalytic subunit. To do this, we have mapped the residues that exhibit chemical shift changes onto the structure of the yeast protein (Figure 9B). Thus the corresponding residues in the yeast sequence are 286M, 420Q, 425G, 427A, 428T and 430N. As can been seen in the figure the residues involved in binding to ilvN form a contiguous surface at the interface of the α−β domains within a catalytic subunit. Although there exists a low sequence identity for these residues between the two proteins, they are present in structurally conserved regions, in that residues 18E (286M), 147D (427A), 148D (428T) and 150V (430N) lie in the alpha-helical segments whereas residues 140H (420Q) and 145A (425G) lie in the loop regions of the two proteins. The structural implication of the binding of ilvN to ilvBβ and ilvBα will be discussed below.

DISCUSSION

Understanding the structural basis for the regulation of the biosynthesis of branched chain amino acids is important from the viewpoint of developing newer antibacterials (*58*) on one hand and for biotechnological production of these essential amino acids for food and pharmaceutical industries (*59*, *60*).

Formation of catalytic sites through subunit association is a common theme for many enzymes (*61*−*63*). AHAS offers a striking example of an enzyme in which binding of essential cofactor TPP requires that independent domains in each monomer associate in the multimeric holoenzyme to form the catalytic site. Biophysical and structural characterization of domains of ilvB and ilvN has shown that the regulatory subunit interacts strongly with the FAD binding domain of ilvB. The regulatory subunit also interacts, although weakly, with the ilvBα domain. Evidence for this comes from both the changes in the CD spectrum and also solution NMR studies. The changes in the NMR spectrum of ilvBβ upon binding ilvN have enabled us to identify the residues involved in this interaction. It should be noted that obtaining sequence specific resonance assignments for this domain has proved to be a challenging task, given that under standard conditions of buffer and salt the protein tends to aggregate and that suitable NMR spectra could only be obtained upon inclusion of the imino acid proline in the

buffer. The ability of proline to aid in stabilizing proteins has been reported previously (*64*, *65*). Here we have shown that proline prevents aggregation of proteins even at concentrations normally employed for solution NMR studies (i.e., >4 mg mL^{-1} for 20 kDa protein).

From an enzymatic point of view, it is interesting to note that ilvBα and ilvBγ domains associate in the presence of TPP and catalyze the formation of acetolactate. The addition of ilvBβ or ilvN only marginally increases the activity of the enzyme. A surprising feature is that the addition of ilvN to the reaction mixture containing all these domains has a marked effect on the enzyme reaction. The stoichiometry in which the reassembled domains interact is not known. The crystal structure of the yeast catalytic subunit shows that extensive inter-subunit and intra-subunit domain−domain interactions exist. However, ilvBβ has almost no structural interaction with either the α or γ domains across the subunit interface. Furthermore it does not have any interactions with the ilvBβ domain across the subunit interface. The increase in enzyme activity could be explained if one considered that the ilvBα and ilvBβ interactions in the complex are similar to the interactions between these domains in the native enzyme.

The role of FAD in AHAS has been inferred to be a structural one, i.e., it is necessary for providing the appropriate geometry for catalysis to occur. The large flexible loops that connect ilvBβ to α and γ domains within a subunit suggest that important domain movement may result upon binding of the regulatory subunit. The binding of ilvN most likely results in bringing the isoalloxazone ring of the bound FAD, which is $\sim$8 Å away from the thiazolium ring of the TPP, closer to the active site thereby providing additional steric factors that enhance enzymatic activity.

As mentioned above, the known regulatory subunits of AHAS are varied in sequence and size. Thus while the effect of binding of regulatory subunit to the catalytic subunit may result in the conformational changes, as shown, it still does not shed any information on the mechanism of feedback inhibition by end products of the metabolic pathway.

More detailed structural investigation, particularly on ilvN alone and in complex with ilvBβ and/or ilvBα and in the presence of valine, will provide some insight into the mechanism of regulation of this protein.

In conclusion, we have studied the interactions between the regulatory subunit and individual domains of the catalytic subunit of *E. coli* AHAS I. NMR resonance assignments have been obtained for the apo form of the FAD binding ilvBβ domain of *E. coli* ilvB. Chemical shift mapping and circular dichroism studies have shown that ilvN interacts with ilvBα and ilvBβ. Using the yeast crystal structure as a model, we propose that the binding of ilvN to ilvBα and ilvBβ could lead to conformational changes that result in observed changes in enzymatic activity. Efforts to determine the high-resolution structure of ilvN are being attempted in order to gain a better understanding of this enzyme.

ACKNOWLEDGMENT

The NMR and Mass Spectrometric Facilities at the Indian Institute of Science are funded from grants by DBT and DST. The authors thank Shaktimala and Mahendran for help in preparing the clones of the domains of ilvB.

SUPPORTING INFORMATION AVAILABLE

Four figures showing protein expression and purification, NMR sample preparation conditions, CD spectrum of the product of the enzyme reaction and table of NMR data acquisition parameters. This material is available free of charge via the Internet at http://pubs.acs.org.

REFERENCES

1. Umbarger, H. E., and Brown, B. (1958) Isoleucine and valine metabolism in *Escherichia coli*, *J. Biol. Chem. 233*, 1156−1160.
2. Chipman, D. M., Duggleby, R. G., and Tittmann, K. (2005) Mechanisms of acetohydroxyacid synthases, *Curr. Opin. Chem. Biol. 9*, 475−481.
3. Chipman, D. M., Barak, Z., and Schloss, J. V. (1998) Biosynthesis of 2-aceto-2-hydroxy acids: acetolactate synthases and acetohydroxyacid synthases, *Biochim. Biophys. Acta 1385*, 401−419.
4. Umbarger, H. E. (1987) Biosynthesis of Branched-Chain Amino Acids, in *Escherichia coli and Salmonella typhimurium: Cellular and Molecular Biology* (Neidhardt, F. C., Ed.) pp 352−367, American Society for Microbiology, Washington, DC.
5. Barak, Z., Chipman, D. M., and Gollop, N. (1987) Physiological implications of the specificity of acetohydroxy acid synthase isozymes of enteric bacteria, *J. Bacteriol. 169*, 3750−3756.
6. Dailey, F. E., and Cronan, J. E. J. (1986) Acetohydroxy acid synthase I, a required enzyme for isoleucine and valine biosynthesis in *Escherichia coli* K-12 during growth on acetate as the sole carbon source, *J. Bacteriol. 165*, 453−460.
7. Eoyang, L., and Silverman, P. M. (1984) Purification and subunit composition of acetohydroxyacid synthase I from *Escherichia coli* K-12, *J. Bacteriol. 157*, 184−189.
8. Hill, C. M., Pang, S. S., and Duggleby, R. G. (1997) Purification of *Escherichia coli* acetohydroxyacid synthase isoenzyme II and reconstitution of active enzyme from its individual pure subunits, *Biochem. J. 327*, 891−898.
9. Vyazmensky, M., Sella, C., Barak, Z., and Chipman, D. M. (1996) Isolation and characterization of subunits of acetohydroxy acid synthase isozyme III and reconstitution of the holoenzyme, *Biochemistry 35*, 10339−10346.
10. Grimminger, H., and Umbarger, H. E. (1978) Acetohydroxy acid synthase I of *Escherichia coli*: purification and properties, *J. Biol. Chem. 137*, 846−853.
11. Davis, E. J., Blatt, J. M., Henderson, E. K., Whittaker, J. J., and Jackson, J. H. (1977) Valine-sensitive acetohydroxy acid synthases in *Escherichia coli* K-12: Unique regulation modulated by multiple genetic sites, *Mol. Gen. Genet. 156*, 239−249.
12. Vinogradov, V., Vyazmensky, M., Engel, S., Belenky, I., Kaplun, A., Kryukov, O., Barak, Z., and Chipman, D. M. (2006) Acetohydroxy acid synthase isozyme I from *Escherichia coli* has unique catalytic and regulatory properties, *Biochim. Biophys. Acta 1760*, 356−363.
13. Favre, R., Wiater, A., Puppo, S., Iaccarino, M., Noelle, R., and Freundlich, M. (1976) Expression of a valine-resistant acetolactate synthase activity mediated by the ilv O and ilv G genes of *Escherichia coli* K-12, *Mol. Gen. Genet. 143*, 243−252.
14. Wek, R. C., Hauser, C. A., and Hatfield, G. W. (1985) The nucleotide sequence of the ilvBN operon of *Escherichia coli*: sequence homologies of the acetohydroxy acid synthase isozymes, *Nucleic Acids Res. 13*, 3995−4010.
15. Lawther, R. P., Wek, R. C., Lopes, J. M., Perira, R., Taillon, B. E., and Wesley, G. (1987) The complete nucleotide sequence of the ilvGMEDA Operon of *Escherichia Coli* K-12, *Nucleic Acids Res. 15*, 2137−2155.
16. Squires, C. H., DeFelice, M., Devereux, J., and Calvo, J. M. (1983) Molecular structure of ilvIH and its evolutionary relationship to ilvG in *Escherichia coli* K12, *Nucleic Acids Res. 11*, 5299−5313.
17. Eoyang, L., and Silverman, P. M. (1986) Role of small subunit (IlvN polypeptide) of acetohydroxyacid synthase I from *Escherichia coli* K-12 in sensitivity of the enzyme to valine inhibition, *J. Bacteriol. 166*, 901−904.
18. Vyazmensky, M., Elkayam, T., Chipman, D. M., and Barak, Z. (2000) Isolation of subunits of acetohydroxy acid synthase III and reconstitution of holoenzyme, *Methods Enzymol. 324*, 95−203.

19. Pang, S. S., and Duggleby, R. G. (1999) Expression, purification, characterization, and reconstitution of the large and small subunits of yeast acetohydroxyacid synthase, *Biochemistry 38*, 5222−5231.
20. Lee, Y., and Duggleby, R. G. (2001) Identification of the regulatory subunit of *Arabidopsis thaliana* acetohydroxyacid synthase and reconstitution with its catalytic subunit, *Biochemistry 40*, 6836−6844.
21. Gollop, N., Damri, D., Barak, Z., and Chipman, D. M. (1989) Kinetics and mechanism of acetohydroxy acid synthase isozyme III from *Escherichia coli*, *Biochemistry 28*, 6310−6317.
22. Pang, S. S., Duggleby, R. G., and Guddat, L. W. (2002) Crystal structure of yeast acetohydroxyacid synthase: A target for herbicidal inhibitors, *J. Mol. Biol. 317*, 249−262.
23. Pang, S. S., Guddat, L. W., and Duggleby, R. G. (2001) Crystallization of the catalytic subunit of *Saccharomyces cerevisiae* acetohydroxyacid synthase, *Acta Crystallogr. D57*, 1321−1323.
24. Kaplun, A., Vyazmensky, M., Zherdev, Y., Belenky, I., Slutzker, A., Mendel, S., Barak, Z., Chipman, D. M., and Shannan, B. (2006) Structure of the regulatory subunit of acetohydroxy acid synthase isozyme III from *Escherichia coli*, *J. Mol. Biol. 357*, 951−963.
25. Mendel, S., Elkayam, T., Sella, C., Vinogradov, V., Vyazmensky, M., Chipman, D. M., and Barak, Z. (2001) Acetohydroxyacid synthase:A proposed structure for the regulatory subunits supported by evidence from mutagenesis, *J. Mol. Biol. 307*, 465−477.
26. Mendel, S., Vinogradov, V., Vyazmensky, M., Chipman, D. M., and Barak, Z. (2003) The N-terminal domain of the regulatory subunit is sufficient for complete activation of acetohydroxyacid synthase III from *Escherichia coli*, *J. Mol. Biol. 325*, 275−284.
27. Vyazmensky, M., Engel, S., Kryukov, O., Berkovich-Berger, D., and Kaplun, L. (2006) Construction of an active acetohydroxyacid synthase I with a flexible linker connecting the catalytic and the regulatory subunits, *Biochim. Biophys. Acta 1764*, 955−960.
28. Mitra, A., Chakrabarti, K. S., Hameed, M. S. S., Srinivas, K. V., Kumar, G. S., and Sarma, S. P. (2005) High level expression of peptides and proteins using cytochrome b_5 as a fusion host, *Protein Expression Purif. 41*, 84−97.
29. Mori, S., Abeygunawardana, C., Johnson, M. O., and Zijl, P. C. M. V. (1995) Improved sensitivity of HSQC spectra of exchanging protons at short interscan delays using a new fast HSQC (FHSQC) detection scheme that avoids water saturation, *J. Magn. Reson. B 108*, 94−98.
30. Piotto, M., Saudek, V., and Sklenar, V. (1992) Gradient-tailored excitation for single-quantum NMR spectroscopy of aqueous solutions, *J. Biomol. NMR 2*, 661−665.
31. Shan, X., Gardner, K. H., Muhandiram, D. R., Rao, N. S., Arrowsmith, C. H., and Kay, L. E. (1996) Assignment of ^{15}N, $^{13}C^{\alpha}$, $^{13}C^{\beta}$, and HN resonances in an ^{15}N, ^{13}C, ^{2}H, labelled 64 kDa Trp repressor−operator complex using triple-resonance NMR spectroscopy and ^{2}H-decoupling, *J. Am. Chem. Soc. 118*, 6570−6579.
32. Wittekind, M., and Mueller, L. (1993) HNCACB, a high-sensitivity 3D NMR experiment to correlate amide-proton and nitrogen resonances with the alpha- and beta-carbon resonances in proteins, *J. Magn. Reson. B 101*, 201−205.
33. Grzesiek, S., and Bax, A. (1992) Improved 3D triple-resonance NMR techniques applied to a 31 kDa protein, *J. Magn. Reson. 96*, 432−440.
34. Muhandiram, D. R., and Kay, L. E. (1994) Gradient-enhanced triple-resonance three-dimensional NMR experiments with improved sensitivity, *J. Magn. Reson. 193*, 203−216.
35. Pervushin, K. (2000) Impact of Transverse Relaxation Optimized Spectroscopy (TROSY) on NMR as a technique in structural biology, *Q. Rev. Biophys. 33*, 161−197.
36. Salzmann, M., Pervushin, K., Wagner, G., Senn, H., and Wuthrich, K. (1998) TROSY in triple-resonance experiments: New perspectives for sequential NMR assignment of large proteins, *Proc. Natl. Acad. Sci. U.S.A. 95*, 13585−13590.
37. Eletsky, A., Kienhöfer, A., and Pervushin, K. (2001) TROSY NMR with partially deuterated proteins, *J. Biomol. NMR 20*, 177−180.
38. Marion, D., Ikura, M., Tschudin, R., and Bax, A. (1989) Rapid recording of 2D NMR spectra without phase cycling. Application to the study of hydrogen exchange in proteins, *J. Magn. Reson. 85*, 393−399.
39. Marion, D., Kay, L. E., Sparks, S. W., Torchia, D. A., and Bax, A. (1988) Three-Dimensional Heteronuclear NMR of ^{15}N-Labeled Proteins, *J. Am. Chem. Soc. 111*, 1515−1517.
40. Delaglio, F., Grzesiek, S., Vuister, G. W., Zhu, G., Pfeifer, J., and Bax, A. (1995) NMRPipe: a multidimensional spectral processing system based on UNIX pipes, *J. Biomol. NMR 6*, 277−293.
41. Kraulis, P. J. (1989) ANSIG: a program for the assignment of protein 1H 2D NMR spectra by interactive graphics, *J. Magn. Reson. 84*, 627−633.
42. Kraulis Domaille, P. J., Campbell-Burk, S. L., Van Aken T., and Laue, E. D. (1994) Solution structure and dynamics of ras p21.GDP determined by heteronuclear three- and fourdimensional NMR spectroscopy, *Biochemistry 33*, 3515−3531.
43. Humphrey, W., Dalke, A., and Schulten, K. (1996) VMD - Visual Molecular Dynamics, *J. Mol. Graphics 14*, 33−38.
44. Koradi, R., Billeter, M., and Wüthrich, K. (1996) MOLMOL: a program for display and analysis of macromolecular structures, *J. Mol. Graphics 14*, 51−55.
45. Westerfeld, W. W. (1945) A colorimetric determination of blood acetoin, *J. Biol. Chem. 161*, 495−502.
46. Epelbaum, S., Chipman, D. M., and Barak, Z. (1990) Determination of products of acetohydroxy acid synthase by the colorimetric method, revisited, *Anal. Biochem. 191*, 96−99.
47. Vinogradov, M., Kaplun, A., Vyazmensky, M., Engel, S., Globik, R., Tittmann, K., Uhlemann, K., Meshalkina, L., Barak, L., Hubner, G., and Chipman, D. M. (2005) Monitoring the acetohydroxy acid synthase reaction and related carboligations by circular dichroism spectroscopy, *Anal. Biochem. 342*, 126−133.
48. Nemeria, N., Tittmann, K., Joseph, E., Zhou, L., Vazquez-Coll, M. B., Arjunan, P., Hubner, G., Furey, W., and Jordan, F. (2005) Glutamate 636 of the *Escherichia coli* pyruvate dehydrogenase-E1 participates in the active center communication and behaves as an engineered acetolactate synthase with unusual stereoselectivity, *J. Biol. Chem. 280*, 21473−21482.
49. Golovanov, A. P., Hautbergue, M. G., Wilson, A. S., and Lian, L. (2004) A simple method for improving protein solubility and long-term stability, *J. Am. Chem. Soc. 126*, 8933−8939.
50. Anglister, J., Grzesiek, S., Ren, H., Klee, C. B., and Bax, A. (1993) Isotope-edited multidimensional NMR of calcineurin B in the presence of the non-deuterated detergent CHAPS, *J. Biomol. NMR 3*, 121−126.
51. Clore, G. M., Wingfield, P. T., and Gronenborn, A. M. (1991) High-resolution three-dimensional structure of Interleukin 1β in solution by three- and four-dimensional Nuclear Magnetic Resonance Spectroscopy, *Biochemistry 30*, 2315−2323.
52. Muchmore, S. W., Sattler, M., Liang, H., Meadows, R. P., Harlan, J. E., Yoon, H. S., Nettesheim, D., Chang, B. S., Thompson, C. B., Wong, S. L., Ng, S. C., and Fesik, S. W. (1996) X-ray and NMR structure of human Bcl-x_l, an inhibitor of programmed cell death, *Nature 381*, 335−341.
53. Wang, G., Peterkofsky, A., Keifer, P. A., and Li, X. (2005) NMR characterization of the *Escherichia coli* nitrogen regulatory protein IIA Ntr in solution and interaction with its partner protein, Npr, *Protein Sci. 14*, 1082−1090.
54. Pérez-Cañadillas, J. M., Santoro, J., Campos-Olivas, R., Lacadena, J., Pozo, A. M., Gavilanes, J. G., Rico, M., and Bruix, M. (2000) The highly refined solution structure of the cytotoxic ribonuclease α-Sarcin reveals the structural requirements for substrate recognition and ribonucleolytic activity, *J. Mol. Biol. 299*, 1061−1073.
55. Sperat, S., and Bax, A. (1991) Empirical correlation between protein backbone conformation and C^{α} and C^{β} ^{13}C Nuclear Magnetic Resonance chemical shifts, *J. Am. Chem. Soc. 113*, 5490−5492.
56. Abell, L. M., and J. V. Schloss. (1991) Oxygenase side reactions of acetolactate synthase and other carbanion-forming enzymes, *Biochemistry 30*, 7883−7887.
57. Tse, J. M. T., and Schloss, J. V. (1993) The oxygenase reaction of Acetolactate Synthase, *Biochemistry 32*, 10398−10403.
58. Grandoni, J. A., Peter, M. T., and Schloss, J. V. (1998) Inhibitors of branched-chain amino acid biosynthesis as potential antituberculosis agents, *J. Antimicrob. Chemother. 42*, 475−482.
59. Sahm, H., and Eggeling, L. (1999) Construction of L-Isoleucine overproducing strains of *Corynebacterium glutamicum*, *Naturwissenschaften 86*, 33−38.
60. Eggeling, I., Cordes, C., Eggeling, L., and Sahm, H. (1987) Regulation of acetohydroxy acid synthase in *Corynebacterium glutamicum* during fermentation of α-ketobutyrate to L-isoleucine, *Appl. Microbiol. Biotechnol. 25*, 346−351.
61. Kang, C., Kim, S., and Fromm, H. J. (1998) Subunit complementation of *Escherichia coli* Adenylosuccinate Synthetase, *J. Biol. Chem. 271*, 29722−29728.

62. Wente, S. R., and Schachman, H. K. (1987) Shared active sites in oligomeric enzymes: Model studies with defective mutants of aspartate transcarbamoylase produced by site-directed mutagenesis, *Proc. Natl. Acad. Sci. U.S.A. 84*, 31−35.

63. Tarun, A. S., and Theologis, A. (1998) Complementation analysis of mutants of 1-aminocyclopropane-1-carboxylate synthase reveals the enzyme is a dimer with shared active sites, *J. Biol. Chem. 20*, 12509−12514.

64. Schobert, B., and Tschesche, H. (1978) Unusual solution properties of proline and its interaction with proteins, *Biochim. Biophys. Acta 541*, 270−277.

65. Samuel, D., Kumar, T. K., Ganesh, G., Jayaraman, G., Yang, P. W., Chang, M. M., Trivedi, V. D., Wang, S. L., Hwang, K. C., Chang, D. K., and Yu, C. (2000) Proline inhibits aggregation during protein refolding, *Protein Sci. 9*, 344−352.

BI701893B